STATISTICS, OPTIMIZATION AND INFORMATION COMPUTING
Stat., Optim. Inf. Comput., Vol. **14**, December 2025, pp 3651–3666.
Published online in International Academic Press (www.IAPress.org)

Parabolic problem considering advection piecewise constant refer to domain using FEM.

Guillermo Villa Martínez*, Carlos Alberto Ramírez Vanegas, José Rodrigo González Granada

Department of Mathematics, Universidad Tecnológica de Pererira, Colombia

Abstract This paper presents a numerical solution of the one-dimensional heat equation using the Finite Element Method (FEM) with time discretization through the implicit Euler scheme. The formulation considers piecewise constant diffusion coefficients over the spatial domain and employs a weak formulation approach for numerical approximation. The study provides a detailed analysis of the assembly process, including mass, stiffness, and load matrices. The Numerical results illustrate the accuracy and stability of the proposed method under different initial conditions and diffusion parameters.

Keywords finite element method, finite element analysis, partial differential equation, heterogeneous domain, parabolic, piecewise constant, problem, weak formulation, discretization, assembly, reference element, Gaussian quadrature.

AMS 2010 subject classifications 65M60

DOI: 10.19139/soic-2310-5070-2490

1. Introduction

The partial differential equation known as the heat equation models the temporal distribution of a quantity [1, 2], such as heat or an electrical current field, in a homogeneous and isotropic solid medium $\Omega : [0,1] \times [0,t_f]$.

$$\frac{\partial u}{\partial t} + \gamma \frac{\partial u}{\partial x} - k(x)\frac{\partial^2 u}{\partial x^2} = f(x). \tag{1}$$

Given boundary conditions:

$$u(0,t) = u(1,t) = 0, \quad t \in [0,t_f], \tag{2}$$

and initial conditions:

$$u(x,0) = g(x). \tag{3}$$

Assume only convection is present. Convection refers to transfer heat from the movement of a medium carrying thermal energy. Fluid (potential) travelling towards point A carries thermal energy from low potential to high potential [1, 3]. Thus, temperature at A will decrease: $\frac{\partial u}{\partial t} < 0$ at A. Conversely, if $\gamma < 0$, fluid travelling left, potential at A will increase. When $\gamma > 0$, fluid travelling right, fluid travelling towards B carries thermal energy from higher to lower potential. Thus, temperature at B will increase: $\frac{\partial u}{\partial t} > 0$ at B. On the other hand, if $\gamma < 0$,

*Correspondence to: Guillermo Villa Martínez (Email: gvilla@utp.edu.co). Department of Department of Mathematics, Universidad Tecnológica de Pererira, Carrera 27 #10-02 Barrio Alamos - Pereira - Risaralda - Colombia (660003).

ISSN 2310-5070 (online) ISSN 2311-004X (print)

fluid travelling towards B carries thermal energy from lower to higher temperature so $\frac{\partial u}{\partial t} < 0$ at B. Therefore, $\frac{\partial u}{\partial t}$ depends on γ and $\frac{\partial u}{\partial x}$. This dependence is negative. Thus, when only convection is present:

$$\frac{\partial u}{\partial t} + \gamma \frac{\partial u}{\partial x} = f(x). \tag{4}$$

If diffusion is also included, then heat equation with advection:

$$\frac{\partial u}{\partial t} + \gamma(x) \frac{\partial u}{\partial x} - \kappa(x) \frac{\partial^2 u}{\partial x^2} = f(x). \tag{5}$$

1.1. Notation

- $u(x,t)$ physical quantity.
- $\frac{\partial u}{\partial t}$ partial derivative with respect to time.
- $\frac{\partial u}{\partial x}$ partial derivative of the displacement.
- $\frac{\partial^2 u}{\partial x^2}$ second partial derivative of the displacement.
- $\varphi(x)$ test function.
- $f(x)$ forcing term.
- $\gamma(x)$: advection term.
- $\kappa(x)$: diffusion term.
- ξ_i Gauss points.
- ω_i Gauss weights.

$u(x,t)$ is the unknown function, representing a physical quantity such as concentration, temperature, or density, depending on position x and time t. $\frac{\partial u}{\partial t}$ the temporal derivative, describing how the quantity u changes over time at a fixed location. It models accumulation or depletion. $\gamma(x)\frac{\partial u}{\partial t}$ is the advection term, which models the transport of u due to a constant velocity $\gamma(x)$. It represents movement with the flow.$\kappa(x)\frac{\partial^2 u}{\partial x^2}$ is the diffusion term, where $\kappa(x)$ is the diffusion coefficient. It models the spreading of u from high to low concentration areas. $f(x)$ is the source term, representing external sources or sinks that either add to or remove from the quantity u at location x.

1.2. Organization

In the preliminaries section, the weak formulation of the second-order parabolic problem is introduced, followed by the derivation of the Galerkin projection using linear elements. Then, the assembly process for the mass, stiffness, and convection matrices is described. Next, numerical experiments are carried out to evaluate the convergence of the solution. Additionally, the functional minimization approach is applied to determine the optimal transport term under different finite element discretizations. Finally, conclusions are presented regarding the accuracy and computational performance of the method.

2. Basic algorithm and extensions

Heat transfer refers to the flow of thermal energy due to differences in the potential of objects. One of the most popular approaches for doing heat transfer analysis is using the finite element method (FEM). We will analyze the solution of a parabolic partial differential equation using the finite element method.

2.1. Test functions

Weak formulation: To create a weak form from a strong form the following steps are summed up.

1. Multiply the strong form by a test function φ and integrate over the entire domain.
2. Integrate by parts

Instead of directly using the strong form of a differential equation in the FEM, one must first reformulate it into the weak (or variational) form.

$$\begin{cases} -\dfrac{d}{dx}\left(k\dfrac{du}{dx}\right) = f(x) \quad ;\forall x \in [0, L] \\ u(0) = u(L) = 0, \end{cases} \tag{6}$$

From the strong form, it is possible to obtain the residual function.

$$r(x) = f(x) + \frac{d}{dx}\left(k\frac{du}{dx}\right) = 0 \tag{7}$$

For all $\forall x \in [0, L]$, the strong form is required to hold. The central concept of the weak form is to convert this point-wise residual into an average, and as outlined by (acá va una referencia), we initiate the process by constructing an integral equation [4].

$$\int_0^L r(x)dx = 0 \tag{8}$$

Defining the weak form through a collection of arbitrarily many integral functions proves unwieldy and restrictive, so we opt to multiply the residual by a function v that is non-zero only in a narrow region. This function, known as the test function (or weight function), is arbitrary (in fact, there are infinitely many such functions) and must equal zero at the boundary where the solution is specified (for example, $v(0) = 0$) [5]. The solution $u(x)$ is part of this same set of functions and is therefore also called the trial function. We are now able to integrater $r(x)v(x)$ over the complete domain $[0, L]$ for different choices of $v(x)$.

$$\int_0^L r(x)v(x)dx = 0 \quad \forall v : v(0) = v(L) = 0. \tag{9}$$

The statement $\forall v : v(0) = v(L) = 0$ above conveys that for all functions v that are zero at $x = 0$, the integral must hold true. This indicates that the test functions must be chosen to vanish at the boundary where the solution u is specified, ensuring the boundary conditions are satisfied. We end up with:

$$\int_0^L \left(f(x) + \frac{d}{dx}\left(k\frac{du}{dx}\right)\right) v(x)dx = 0 \tag{10}$$

Now, integrating (10)

$$\int_0^L k\frac{du}{dx}\frac{dv}{dx}dx - \left[k\frac{du}{dx}v\right]_0^L = \int_0^L fvdx, \tag{11}$$

and we end up with the weak form of our model problem:

$$\int_0^L k\frac{du}{dx}\frac{dv}{dx}dx = \int_0^L f(x)v(x)dx \quad \forall v : v(0) = v(L) = 0. \tag{12}$$

On the other hand, the model problem can also be formulated as a minimization problem: find u such that $F(u) \leq F(v)$ for all admissable functions v, where:

$$F(v) = \frac{1}{2}\int_0^L k\left(\frac{dv}{dx}\right)^2 - \int_0^L fvdx \tag{13}$$

The functional F represents the potential energy of the physical system obeying the model problem, and thus the actual solution to our physical problem is the one that minimizes potential energy [6].

3. Parabolic problem

Given the differential equation posed in (5) and a solution $u(x,t)$ of a test space of coersive linear functions, multiply (5) by $v = \varphi_j(x)$:

$$\int_\Omega \frac{\partial u}{\partial t} v dx + \int_\Omega \gamma(x) \frac{\partial u}{\partial x} v dx - \int_\Omega \frac{\partial}{\partial x}\left(\kappa(x)\frac{\partial u}{\partial x}\right) v = \int_\Omega f v dx. \tag{14}$$

Where $u(x,t)$ is given by the linear combination [8, 9]:

$$u(x,t) = \sum_{i=1}^{n+1} \alpha_i(t)\varphi_i(x), \tag{15}$$

deriving (15) with respect to time:

$$\frac{\partial u(x,t)}{\partial t} = \sum_{i=1}^{n+1} \alpha_i'(t)\varphi_i(x), \tag{16}$$

then:

$$\int_\Omega \frac{\partial u}{\partial t} v dx = \int_\Omega \sum_{i=1,j=1}^{n+1} \alpha_i'(t)\varphi_i(x)\varphi_j(x)dx,, \tag{17}$$

with:

$$[M] = m_{ij} = \int_\Omega \varphi_i(x)\varphi_j(x)dx, \quad i,j = 1,2,\ldots,n+1. \tag{18}$$

$\gamma(x)$ is a combination of base elements:

$$\gamma(x) = \sum_{l=0}^{n} \lambda_l \varphi_l(x) \tag{19}$$

where λ_l are constants that depends of transport. Matrix $[A]$ is given by:

$$\int_\Omega \gamma(x)\frac{\partial u}{\partial x} v dx = \sum_{l=0}^{n} \lambda_l \int_\Omega \varphi_l(x)\varphi_i'(x)\varphi_j(x)dx, \tag{20}$$

with:

$$[A] = A_{ij} = \lambda_0 A^0 + \lambda_1 A^1 + \cdots + \lambda_n A^0 \tag{21}$$

The superindex indicates the calculation of (20) for each element. Assuming that the diffusion terms are constant from element to element:

$$-\kappa \int_\Omega \frac{\partial}{\partial x}\left(\frac{\partial u}{\partial x}\right) v dx = -\kappa \int_\Omega \frac{\partial u}{\partial x}\frac{\partial v}{\partial x} dx = -\kappa \int_\Omega \sum_{i=1,j=1}^{n+1} \alpha_i(t)\varphi_i'(x)\varphi_j'(x)dx, \tag{22}$$

where:

$$[S] = S_{ij} = \kappa \int_\Omega \varphi_i'(x)\varphi_j'(x)dx, \quad i,j = 1,2,\ldots,n+1. \tag{23}$$

Finally,

$$\int_{\Omega} f(x)vdx = \int_{\Omega} f(x)\varphi_i(x)dx, \tag{24}$$

then:

$$[B] = b_i = \int_{\Omega} f(x_i)\varphi_i(x)dx \tag{25}$$

Continuing with the derivative in time we have:

$$[M]\frac{\overrightarrow{d\alpha}}{dt} + ([A] + [S])\,\overrightarrow{\alpha} = [B]. \tag{26}$$

Using an implicit Euler scheme,

$$\overrightarrow{\alpha}_m = \left(\frac{1}{\Delta t}[M] + [A] + [S]\right)^{-1}\left([B] + \frac{1}{\Delta t}[M]\overrightarrow{\alpha}_{m-1}\right) \tag{27}$$

For $m = 1, 2, \ldots, n+1$ partitions in time. We acknowledge the concern regarding computational efficiency, particularly for large-scale problems using the implicit Euler scheme and matrix assembly. While our primary focus was on verifying solution accuracy, we addressed the potential performance limitations by conducting a grid convergence study using the Grid Convergence Index (GCI).

3.1. Assembling

To describe any mesh we need a coordinate matrix (vector in 1D)

$$x = [x_1, x_2, \cdots, x_n]^t \tag{28}$$

and a nodal connectivity matrix,

$$[T] = \begin{bmatrix} 1 & 2 \\ 2 & 3 \\ \vdots & \vdots \\ n & n+1 \end{bmatrix}, \tag{29}$$

and linear n elements will lead $n+1$ equations to be solved for φ_i, $i = 1, 2, \ldots, n+1$,

$$[\varphi] = [\varphi_1, \varphi_2, \ldots, \varphi_{n+1}]^t. \tag{30}$$

An element e netween nodes x_i and x_j contributes only to equation i and j. We can use e' th row of equation (29) to see which nodes are associated with the element e. Now, for each element e we define x_1 and x_2, compute φ as linear combination of linear equation, then compute $[M^e]$, $[A^e]$,$[S^e]$ and $[B^e]$. Element stiffness matrix (18):

$$[M^e] = \begin{bmatrix} \int_{x_1}^{x_2} \varphi_1(x)\varphi_1(x)dx & \int_{x_1}^{x_2} \varphi_1(x)\varphi_2(x)dx \\ \int_{x_1}^{x_2} \varphi_2(x)\varphi_1(xdx) & \int_{x_1}^{x_2} \varphi_2(x)\varphi_2(x)dx \end{bmatrix}. \tag{31}$$

Elements in matrix (23):

$$[S^e] = \kappa \begin{bmatrix} \int_{x_1}^{x_2} \varphi_1'(x)\varphi_1'(x)dx & \int_{x_1}^{x_2} \varphi_1'(x)\varphi_2'(x)dx \\ \int_{x_1}^{x_2} \varphi_2'(x)\varphi_1'(xdx) & \int_{x_1}^{x_2} \varphi_2'(x)\varphi_2'(x)dx \end{bmatrix}, \tag{32}$$

elements in matrix (20)

$$[A^{e_l}] = \begin{bmatrix} \int_{x_1}^{x_2} \varphi_l(x)\varphi_1'(x)\varphi_1(x)dx & \int_{x_1}^{x_2} \varphi_l(x)\varphi_1(x)\varphi_2(x)dx \\ \int_{x_1}^{x_2} \varphi_l\varphi_2'(x)\varphi_1'(xdx) & \int_{x_1}^{x_2} \varphi_l\varphi_2'(x)\varphi_2(x)dx \end{bmatrix}, \tag{33}$$

and element load vector (25):

$$[B^e] = \begin{bmatrix} \int_{x_1}^{x_2} f(x)\varphi_1(x)dx \\ \int_{x_1}^{x_2} f(x)\varphi_1(x)dx \end{bmatrix}, \tag{34}$$

for each element e, we add (31,32,33,34) to correct place in (18,21,23,25). We need to add each element contribution to the global mass matrix:

$$\begin{bmatrix} M_{ii}^{new} \\ M_{ij}^{new} \end{bmatrix} = \begin{bmatrix} M_{ii}^{old} + M_{11}^{e} \\ M_{ij}^{old} + M_{12}^{e} \end{bmatrix} \tag{35}$$

or on matrix form $M(row, col)$, where row denotes the array containing the row indices and col the column indices. Thus we could write $M([i.j], [i, j])$, to mean a sub-matrix M with rows i and j and columns i and j. All nodes that have several elements will get contributions from each element. We are accumulating mass to these nodes from the elements.

3.2. Discussion

The weak formulation presented above is essential for transforming the original partial differential equation into a form suitable for numerical approximation. By multiplying the governing equation by a test function $v \in H_0^1(\Omega)$ and integrating over the domain, the resulting formulation reduces the regularity requirements on the solution and enables the use of variational techniques.

The diffusion term is integrated by parts using the divergence theorem, transferring derivatives from the solution to the test function. Since the test functions vanish on the boundary, the boundary integral drops out. This leads to the definition of the bilinear form $b(u, v)$ associated with diffusion.

Similarly, the advection term is retained in its original form, resulting in the bilinear form $a(u, v)$, while the source term becomes the linear functional $L(v)$. The weak formulation is thus expressed as finding $u \in H_0^1(\Omega)$ such that for all $v \in H_0^1(\Omega)$,

$$\left(\frac{\partial u}{\partial t}, v\right) + a(u, v) + b(u, v) = L(v).$$

This continuous formulation is then discretized using the finite element method (FEM). The domain Ω is divided into a finite set of subdomains (elements), and the solution u_h is approximated using a linear combination of piecewise polynomial basis functions φ_i. The resulting semi-discrete problem leads to a system of ordinary differential equations in time.

The algebraic formulation is expressed as:

$$M\frac{\partial u_h}{\partial t} + (A + S)u_h = B,$$

where:

- $M_{ij} = \int_\Omega \varphi_i\varphi_j \, d\boldsymbol{x}$ is the **mass matrix**.
- $S_{ij} = \int_\Omega \kappa(\boldsymbol{x})\nabla\varphi_i \cdot \nabla\varphi_j \, d\boldsymbol{x}$ is the **stiffness matrix**.

- $A_{ij} = \int_\Omega \gamma(\boldsymbol{x}) \cdot \nabla\varphi_i \, \varphi_j \, d\boldsymbol{x}$ is the **advection matrix**.
- $B_i = \int_\Omega f(\boldsymbol{x}, t)\varphi_i \, d\boldsymbol{x}$ is the **load vector**.

This matrix system is the starting point for implementing time-stepping schemes and solving the full space-time problem numerically.

4. Galerkin orthogonality

Let V be a Hilbert space with norm $||.||_V$. Find $u \in V$ such that:

$$a(u, \varphi) = l(\varphi) \quad \forall \varphi \in V. \tag{36}$$

With the above, the bilinear form of a and the right-hand side functional l depend on the partial differential equation. For Galerkin orthogonality, the following forms are to be considered [7]:

1. The first form consists of the weak formulation, where V is a space of infinite-dimensional functions:
$$a(u, \varphi) = l(\varphi) \quad \forall \varphi \in V.$$
2. The second form is the discrete weak formulation. In this formulation the infinite dimensional function space V is replaced by a finite dimensional subspace V^h [7]:
$$a(u_h, \varphi_h) = l(\varphi_h) \quad \forall \varphi_h \in V^h \subset V.$$

Galerkin orthogonality implies that the error $u - u_h$ is perpendicular to every function within the finite-dimensional space V_h, and this relationship is written as::

$$a(u - u_h, \varphi_h) = 0 \quad \forall \varphi_h \in V^h. \tag{37}$$

To prove Galerkin orthogonality one needs to subtract the previously described forms. Subtracting the weak formulations with a test function $varphi_h \in V^h subset V$ one obtains:

$$a(u, \varphi_h) - a(u_h, \varphi_h) = l(\varphi_h) - l(\varphi_h) = 0.$$

Using the fact that the bilinear form of a is linear in the term of the first argument, one has:

$$a(u - u_h, \varphi_h) = 0 \quad \forall \varphi_h \in V^h.$$

Another approach is to represent the function space V on a plane graph. Assigning the horizontal axis to the subspace V^h allows us to include both the weak formulation solution u and the solution u_h as shown:

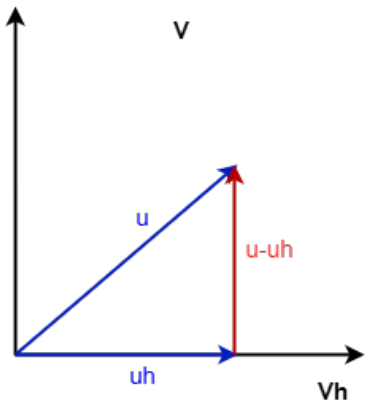

Figure 1. Solution space V, subspace V^h y error $u - u_h$

The vector $u - u_h$ represents the difference between the two solutions and is orthogonal to each $varphi_h$ function present in the bilinear form a. these $varphi_h$ these functions are located on the horizontal axis.

4.1. Céa's Lemma

In this subsection a first error estimator will be found. It is assumed that the variational formulation of the partial differential equation satisfies the following properties:

1. The right-hand side $l(.)$ is a bounded linear form:

$$\exists C > 0 : |l(u)| \leq C||u||_V \quad \forall u \in V.$$

2. $a(.,.)$ is a continuous bilinear form on $V \times V$. [9, 11]:

$$\exists K > 0 : |a(u,v)| \leq K||u||_V||v||_V \quad \forall u, v \in V.$$

3. The bilinear form $a(.,.)$ is coercive:

$$\exists \alpha > 0 : a(u,u) \geq \alpha||u||_V^2 \quad \forall u \in V.$$

So Céa's lemma aims at proving the following inequality [7]:

$$||u - u_h||_V \leq \frac{K}{\alpha} \inf_{\varphi_h \in V_h} ||u - \varphi_h||_V \tag{38}$$

To prove the inequality of the equation (38), of Galerkin orthogonality:

$$a(u - u_h, w_h) = 0 \quad \forall w_h \in V_h.$$

You select $w_h = u_h - \varphi_h$ and you get:

$$\alpha||u - u_h||^2 \leq a(u - u_h, u - u_h) = a(u - u_h, u - u_h) + a(u - u_h, u_h - \varphi_h).$$

Adding $a(u - u_h, u_h - \varphi_h) = 0$ does not affect the initial inequality. Taking advantage of the bilinear form and the linearity in the second component we have:

$$\alpha||u - u_h||^2 \leq a(u - u_h, u - u_h) = a(u - u_h, u - \varphi_h).$$

Applying continuity of the bilinear form [8, 10],

$$\alpha||u - u_h||^2 \leq K||u - u_h||||u - \varphi_h||.$$

This leads to the following result:

$$||u - u_h|| \leq \frac{K}{\alpha}||u - \varphi_h|| \Rightarrow ||u - u_h|| \leq \frac{K}{\alpha} \inf_{\varphi_h \in V^h} ||u - \varphi_h||.$$

4.2. Grid convergence index

The Grid Convergence Index (GCI) is used to ensure that numerical simulation results are independent of the mesh size, which is a critical aspect of verifying the accuracy of computational models [12]. By providing a quantitative estimate of the discretization error, GCI helps assess how much the numerical solution would change with further mesh refinement. This allows researchers and engineers to determine whether their simulations are sufficiently resolved and in the asymptotic range of convergence [13]. Ultimately, using GCI improves the credibility and reliability of simulation-based studies, particularly in fields like fluid dynamics, structural mechanics, and other areas of engineering and physics where precise numerical predictions are essential. Below is the algorithm for calculating GCI:

Algorithm 1 Grid Convergence Index (GCI) and Richardson Extrapolation

Input: Numerical results on three grids: $f_{\text{coarse}}, f_{\text{med}}, f_{\text{fine}}$
Input: Grid sizes: $h_{\text{coarse}}, h_{\text{med}}, h_{\text{fine}}$
Input: Safety factor F_S (typically 1.25 or 3.0)
Compute grid refinement ratio: $r = \dfrac{h_{\text{coarse}}}{h_{\text{med}}} = \dfrac{h_{\text{med}}}{h_{\text{fine}}}$
Compute relative error ratio: $R_E = \dfrac{|f_{\text{fine}} - f_{\text{med}}|}{|f_{\text{med}} - f_{\text{coarse}}|}$
Compute estimated order of convergence: $p = \dfrac{\ln(1/R_E)}{\ln(r)}$
Compute $GCI_{\text{CM}} = F_S \cdot \left(\dfrac{|f_{\text{med}} - f_{\text{coarse}}|}{f_{\text{med}}(r^p - 1)} \right)$
Compute $GCI_{\text{MF}} = F_S \cdot \left(\dfrac{|f_{\text{fine}} - f_{\text{med}}|}{f_{\text{fine}}(r^p - 1)} \right)$
Compute asymptotic convergence ratio:

$$CAR = r^p \cdot \frac{GCI_{\text{MF}}}{GCI_{\text{CM}}}$$

if $CAR \approx 1$ **then**
    The solution is in the asymptotic range of convergence
    Apply Richardson extrapolation:

$$f_{\text{exact}} \approx f_{\text{fine}} + \frac{f_{\text{fine}} - f_{\text{med}}}{r^p - 1}$$

else
    Further mesh refinement is required
end if

5. Numerical results

We want to solve using FEM a parabolic partial differential equation as in equation (5), considering zero boundary conditions for different scenarios of initial conditions as shown below.

5.1. PDE time dependent

Parameters

- $n = [4, 100]$
- $a = 0$: lower limit
- $L = 1$: upper limit
- $\gamma(x)$: convection piecewise constant
- $k = 0.001$: diffusion constant
- $t_f = 10$: final Time
- $Nt = 100$: time partition
- $dt = tf/Nt$: delta time
- Boundary conditions $u_0 = 0$
- $u_0 = u_0$: Potential at a $u(x = a) = 0$
- $u_1 = u_0$; Potential at $u(x = b) = 0$
- $f(x) = 5(-4(x - 0.5)^2 + 1)$: Forcing term.

5.1.1. Initial condition 1.

$$u(x, 0) = x(1 - x). \tag{39}$$

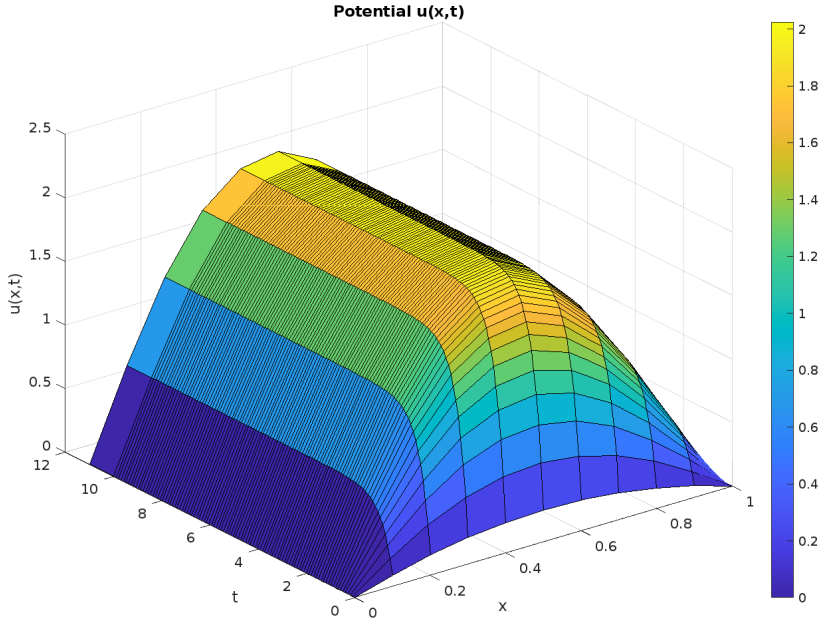

Figure 2. Electrical current at any x point and time t

Evolution of the Distribution. Figure 2 shows the time evolution of the solution $u(x,t)$ over the spatial domain. The color gradient indicates variations, with the highest values appearing in the central region and decreasing towards the boundaries. This visualization highlights the stability of the numerical method applied.

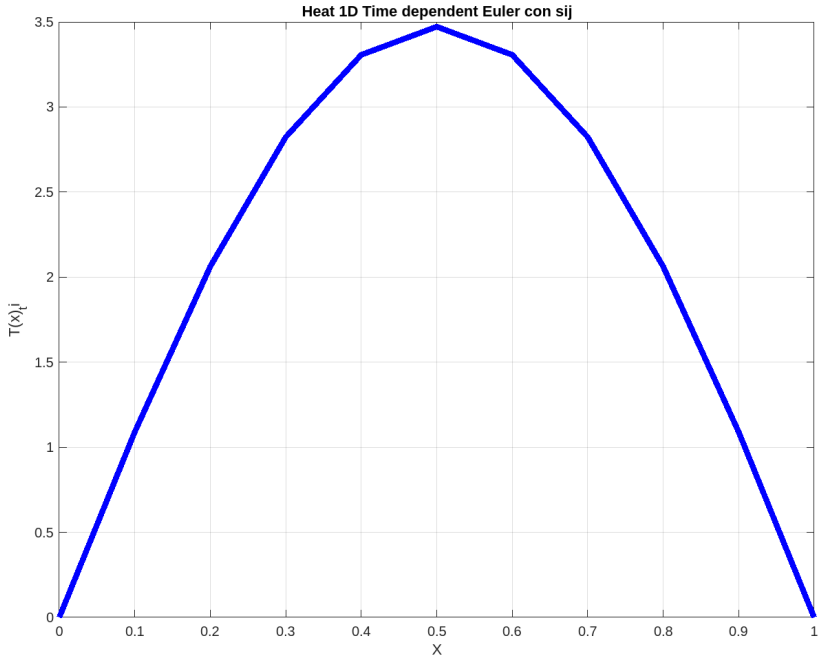

Figure 3. Electrical current at any x point and time t_f

Figure 3 numerical solutions for $u(x,t_f)$ along spatial domain $x \in [0,1]$ neglecting $\gamma(x)$ as piece wise elements.

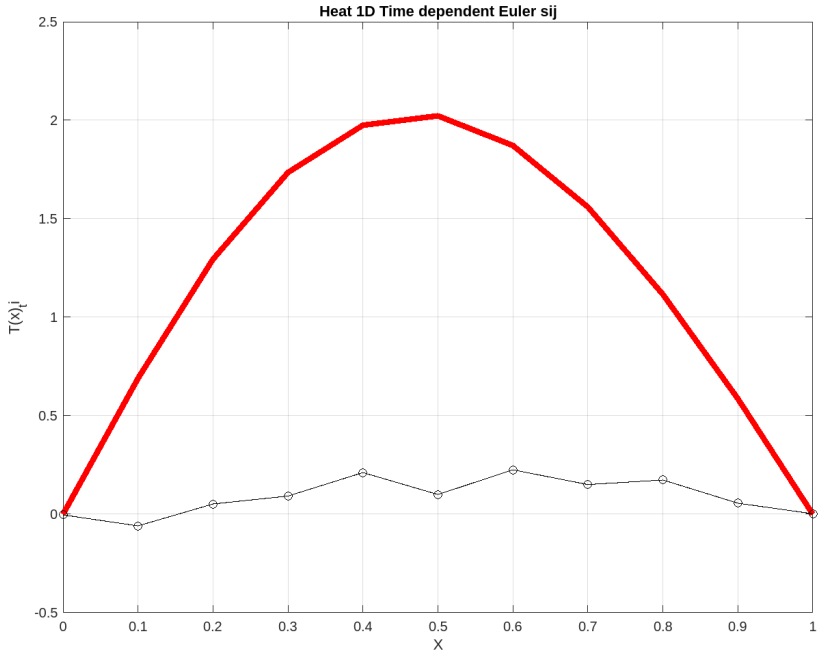

Figure 4. $u(x, t_f)$ at any x point and time t_f with γ_{opt}

Figure 4 represents the evolution of the distribution $u(x, t_f)$ along the spatial domain $x \in [0, 1]$ at final time. The red thick curve corresponds to a specific numerical solution, while the black curve with circles represents an optimal solution for $\gamma(x)$.

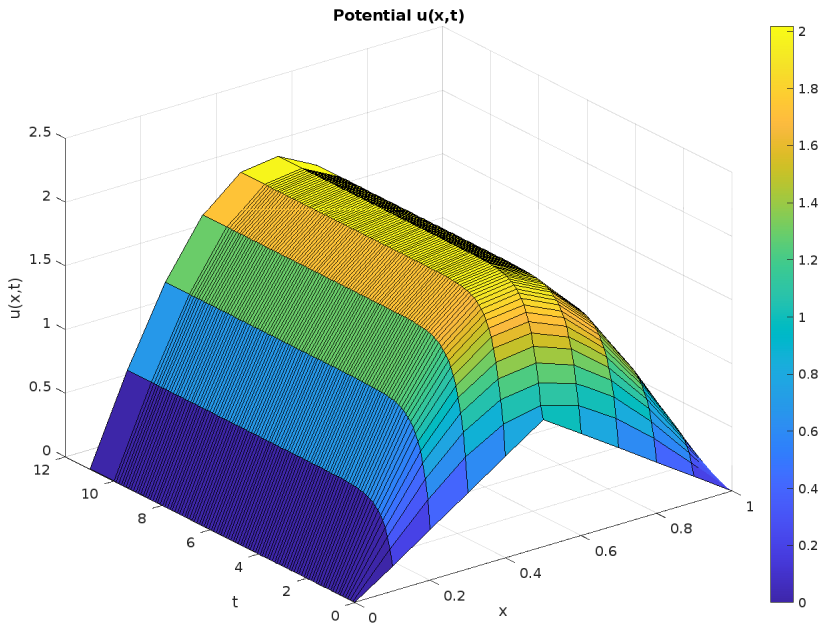

Figure 5. $u(x, t)$ at any x point and time t

5.1.2. Initial condition 2. Considering a piecewise initial condition:

$$u(x,0) = \begin{cases} 2x & ; \quad 0 \leq x < \dfrac{1}{2} \\ \\ 2(1-x) & ; \quad \dfrac{1}{2} \leq x \leq 1 \end{cases} \tag{40}$$

The solution $u(x,t)$ 5 starts from a triangular-shaped initial profile and evolves under the influence of weak diffusion, convection, and a centered forcing term. As time progresses, the solution smooths out and grows in amplitude near the center due to the persistent effect of the source term.

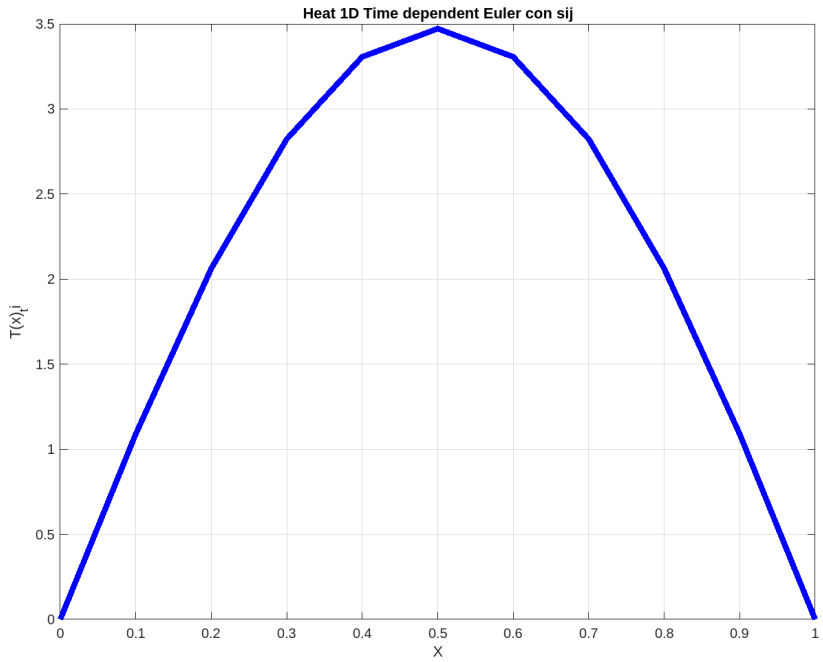

Figure 6. Electrical current at any x point and time t_f

Eventually, $u(x,t_f)$ approaches a steady-state profile where the balance between advection, diffusion, and forcing dominates the dynamics. The boundaries remain fixed at zero due to the homogeneous Dirichlet conditions.

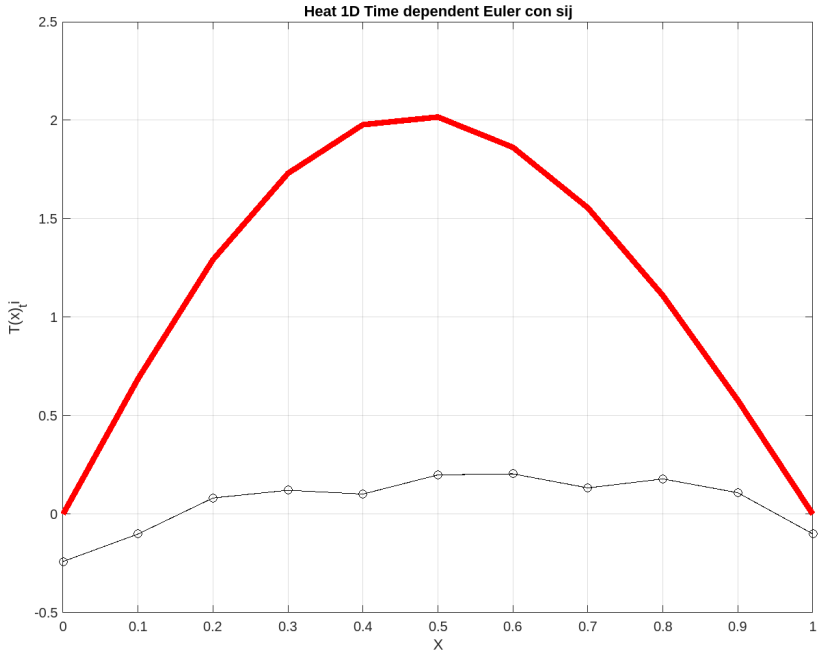

Figure 7. Electrical current at any x point and time t_f with $\gamma(x)_{opt}$

The figure 7 displays the potential $u(x, t_f)$ across the spatial domain at the final time t_f due to optimal convection profile $\gamma(x)_{opt}$

5.1.3. GCI The coarsest mesh refers to the mesh with the largest $(n = 25)$ element size, while the finest mesh corresponds to the one with the smallest element size $(n = 100)$. The mesh spacing represents the average width of the elements. The refinement ratio is defined as the ratio between the element sizes of two successive meshes, specifically from the coarser to the finer mesh. The approximation denotes the predicted value of the quantity of interest at time $t = 0.022$ and position $x = 0.4$; this could represent, for instance, the displacement or stress at a specific point, the total force on a boundary, or the overall energy within the system.

1. Grid refinement ratio:
$$r = \frac{h_3}{h_2} = \frac{h_2}{h_1} = \frac{0.04}{0.02} = 2$$
2. Relative error ratio:
$$R_E = \frac{|f_1 - f_2|}{|f_2 - f_3|} = \frac{|1.3744 - 1.3742|}{|1.3742 - 1.3737|} = \frac{0.0002}{0.0005} = 0.4$$
3. Estimated order of convergence:
$$p = \frac{\ln(1/R_E)}{\ln(r)} = \frac{\ln(1/0.4)}{\ln(2)} \approx \frac{\ln(2.5)}{\ln(2)} \approx 1.3219$$
4. Compute GCI_{CM}:
$$GCI_{CM} = 1.25 \cdot \frac{|f_2 - f_3|}{f_2(r^p - 1)} = 1.25 \cdot \frac{0.0005}{1.3742(2^{1.3219} - 1)} \approx 3.0322 \times 10^{-4}$$
5. Compute GCI_{MF}:
$$GCI_{MF} = 1.25 \cdot \frac{|f_1 - f_2|}{f_1(r^p - 1)} = 1.25 \cdot \frac{0.0002}{1.3744(2^{1.3219} - 1)} \approx 1.2129 \times 10^{-4}$$

6. Compute Asymptotic Convergence Ratio:

$$CAR = r^p \cdot \frac{GCI_{MF}}{GCI_{CM}} = 2^{1.3219} \cdot \frac{1.2129 \times 10^{-4}}{3.0322 \times 10^{-4}} \approx 2.5 \cdot 0.40000659 \approx 0.99999701 \approx 1$$

7. Since $CAR \approx 1$, the solution is in the asymptotic range.
8. Richardson extrapolation:

$$f_{\text{exact}} \approx f_1 + \frac{f_1 - f_2}{r^p - 1} = 1.3744 + \frac{0.0002}{2^{1.3219} - 1} \approx 1.374533$$

9. GCI 95% confidence interval:

$$\text{Lower bound: } f_1 - GCI_{MF} = 1.3744 - 1.2129 \times 10^{-4} = 1.374278$$

$$\text{Upper bound: } f_1 + GCI_{MF} = 1.3744 + 1.2129 \times 10^{-4} = 1.374521$$

GCI	**Value**
Refinement ratio (r)	2
Order of accuracy (p)	1.3219
GCI_{CM}	3.0322×10^{-4}
GCI_{MF}	1.2129×10^{-4}
Asymptotic ratio (CAR)	0.99999701
Estimated true solution	1.374533
95% Confidence Interval (min)	1.374278
95% Confidence Interval (max)	1.374521

Table 1. Final report table using GCI and Richardson extrapolation.

The results indicate that the solution lies within the asymptotic range of convergence, as evidenced by a consistent order of accuracy and a CAR (asymptotic ratio) close to 1. This justifies the use of our current mesh resolution without further refinement.

5.2. Functional $J(\gamma(x))$

Finally, the matlab "fminsearch" command is used to find the optimal values of λ. This consists of, for an initial vector of λ the differential equation (26) is solved and the algorithm advances to update the value of the next λ until a minimum value of the convex functional is found by exhausting the maximum number of iterations.

$$J(\gamma(x)) = \frac{1}{2}\int_{[0,1]\times[0,t_f]} \gamma(x)^2 dxdt + \frac{1}{2}\int_{r\times[0,t_f]} u^2(x,t)dxdt + \frac{1}{2}\int_{[0,1]} u^2(x,t_f)dx \tag{41}$$

The above matrices have the following matrix equivalence:

$$\frac{1}{2}\int_{[0,1]\times[0,t_f]} \gamma(x)^2 dxdt = \frac{1}{2}\left(\lambda^t[M]\lambda\right)t_f \tag{42}$$

λ are th e values of the equation 19 for the formulation of $k(x)$ as piecewise.

$$\frac{1}{2}\int_{r\times[0,t_f]} u^2(x,t)dxdt = \frac{1}{2}\left(\alpha_r^t[M_r]\alpha_r\right)t_f \tag{43}$$

Mass matrix M_r with T elements contained in a subdomain r. Initial values are considered to be zero for $\gamma(x)$.

$$\frac{1}{2}\int_{[0,1]} u^2(x,t_f)dx = \frac{1}{2}\alpha^t(t_f)[M]\alpha(t_f) \tag{44}$$

$\alpha(t_f)$ are the values of the solution of (26) at the final time t_f.

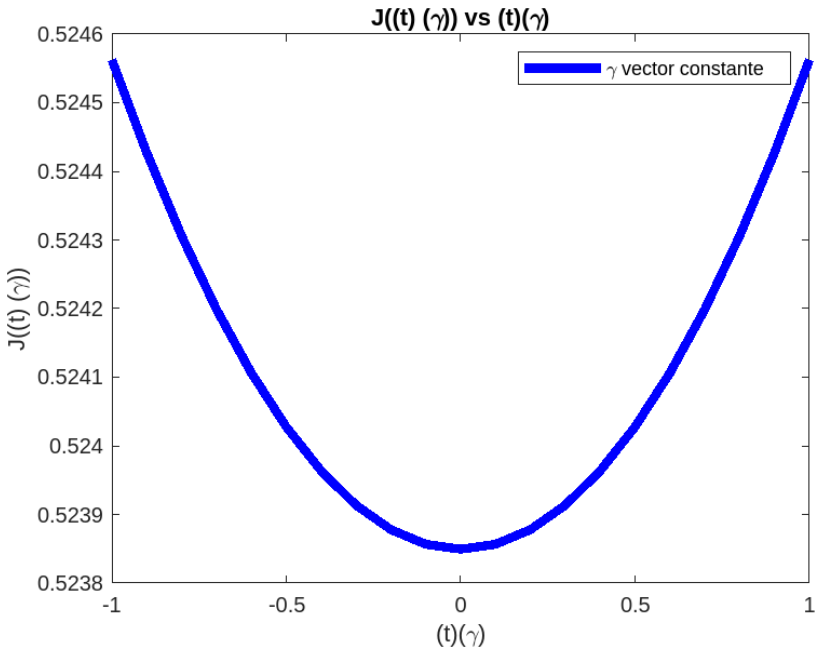

Figure 8. Convex numerical functional $J(\gamma(x))$

Taking two random values of γ, the functional is plotted by evaluating the convexity condition

$$J((1-t)\gamma(x)_i + t\gamma(x)_{i+1}) \leq (1-t)f(\gamma(x)_i) + tf(\gamma(x)_{i+1}), \quad \forall t \in [0,1].$$

For the simulation with 100 elements (finest mesh), a minimum value of the functional $J(\gamma_{opt}) = 0.148554$ was obtained after 10000 iterations with a computational time of 495.8639 seconds.

6. Summary and future work

In this work, we implemented a numerical solution for the one-dimensional heat equation using the Finite Element Method (FEM) with an implicit Euler time-stepping scheme. This equation represents fluid permeability, fluid pressure, or current distribution. The weak formulation allowed us to derive a system of linear equations, which was solved iteratively. The numerical results demonstrated that the method provides stable and accurate solutions, even when dealing with piecewise constant diffusion coefficients and several scenarios for initial conditions. Future research could explore adaptive mesh refinement techniques to enhance computational efficiency. Additionally, incorporating space- or time-dependent convection profiles, nonlinear source terms, or extending the approach to two- and three-dimensional geometries could provide deeper insights into more realistic physical systems.

Acknowledgement

This work was supported by master in mathematic program at Universidad Tecnológica de Pereira.

REFERENCES

1. Li Chen, Veniamin Gvozdik, Yue Li, *Rigorous derivation of the degenerate parabolic-elliptic Keller-Segel system from a moderately interacting stochastic particle system*, Journal of Differential Equations, Volume 375, 2023, Pages 567-617.
2. Susanne C. Brenner and Ridgway Scott, *The Mathematical Theory of Finite Element Methods*, Texts in Applied Mathematics, Springer, 3rd Edition, 2021,
3. Hongliang Liu, Yilin You, Haodong Li, Shoufu Li, *Canonical Euler splitting method for parabolic partial functional differential algebraic equations*, Applied Numerical Mathematics, Volume 190, 2023, Pages 65-83.
4. Markus Bachmayr, Manfred Faldum, *A space-time adaptive low-rank method for high-dimensional parabolic partial differential equations*, Journal of Complexity, Volume 82, 2024, Pages 101-123.
5. Bhushan Prabhune, K. Suresh, *An isoparametric tangled finite element method for handling higher-order elements with negative Jacobian*, Computational Mechanics, Volume 73, 2024, Pages 159-176.
6. Markus Merkel, Andreas Öchsner, *One-Dimensional Finite Elements: An Introduction to the Method*, Springer, 2023.
7. C. Johnson, *Numerical solution of partial differential equations by the finite element method*, Cambridge University Press, Cambridge, 1987.
8. Jim Rulla, *Analysis for Implicit Approximations to Solutions to Cauchy Problems*, SIAM Journal on Numerical Analysis,vol.33, pp. 68-87, 1996.
9. J.Galvis and H. Versieux, *Introdução a Aproximação Numérica de Equações Diferenciais Parciais Via o Método de Elementos Finitos*, Lecture notes for a minicourse in the 28 Colóquio Brasileiro de Matemática IMPA,2011.
10. W. Liao, Mehdi Dehghan, A. Mohebbi, *Direct numerical method for an inverse problem of a parabolic partial differential equation*, Journal of Computational and Applied Mathematics, Volume 232, 2023, Pages 351-361.
11. Larbi Bougoffa, Robert C. Rach, *Solving nonlocal initial-boundary value problems for linear and nonlinear parabolic and hyperbolic partial differential equations by the Adomian decomposition method*, Applied Mathematics and Computation, Volume 225, 2023, Pages 50-61.
12. Yoshihide Tominaga, *CFD simulations of turbulent flow and dispersion in built environment: A perspective review*, Journal of Wind Engineering and Industrial Aerodynamics, Volume 249, 2024, Pages 1-26.
13. Julien Bect, Souleymane Zio, Guillaume Perrin, Claire Cannamela, Emmanuel Vazquez, *On the quantification of discretization uncertainty: comparison of two paradigms*, Journal of Computational Physics (Elsevier), Volume 428, 2021, Pages 110052.